# Spin-orbit and electronic interactions in narrow-gap quantum dots

C. F. Destefani,[1,2] Sergio E. Ulloa,[2] and G. E. Marques[1]
[1]*Departamento de Física, Universidade Federal de São Carlos, 13565-905, São Carlos, São Paulo, Brazil*
[2]*Department of Physics and Astronomy and Nanoscale and Quantum Phenomena Institute, Ohio University, Athens, Ohio 45701-2979, USA*

(Received 3 August 2004; published 11 November 2004)

We present a detailed analysis of spin-orbit couplings in zinc-blende narrow-gap parabolic quantum dots built in the plane of a two-dimensional electron gas. Such couplings are related to both bulk (Dresselhaus) and surface (Rashba) inversion asymmetry terms in the Hamiltonian of the system. We start by focusing on how the pure Fock-Darwin spectrum of an InSb quantum dot is modified by the addition of separate terms of spin-orbit coupling; we then deal with the presence of all spin-orbit terms in the numerical diagonalization of the single-particle model. We also consider a two-electron quantum dot—by antisymmetrizing the one-electron basis—and study the competition between electron-electron and spin-orbit interactions. All these effects are analyzed in the presence of a magnetic field perpendicular to the quantum dot. Selection rules for spin-orbit-induced level anticrossings, as well as critical fields and energy minigaps related to them, zero-field energy splittings, and the role of the *g*-factor on the spectrum are also addressed.

DOI: 10.1103/PhysRevB.70.205315 PACS number(s): 73.21.La, 71.70.Ej, 78.30.Fs

## I. INTRODUCTION

The creation and manipulation of spin populations in semiconductor nanostructures[1] has been receiving growing attention, mainly because of the Datta-Das proposal[2] for a spin field-effect transistor, whose working is based on the Rashba spin-orbit (SO) coupling of the electrons in a two-dimensional electron gas (2DEG). Such a device has practically given origin to spintronics research,[3–5] where not only the charge of electron but also its spin is able to transport information; recently, the inclusion of the Dresselhaus SO coupling in this dispositive has been proposed as an alternative to its original concept.[6] Another reason for the growing interest in spintronics is the possibility of building quantum computation devices, whose working is based on a coherent superposition of states in a two-level system by using, for example, quantum dots (QDs).[7–9] For those reasons, a clear understanding of spin relaxation mechanisms[10–13] caused, among others, by SO effects, is essential. Studies about the distinct SO couplings are carried out, for example, in quantum wells in Refs. 14 and 15, in heterostructures in Refs. 16 and 17, and in zinc-blende nanocrystals in Ref. 18. In this work, we are interested in the SO effects induced in the Fock-Darwin (FD) spectrum of parabolic zinc-blende narrow-gap QDs defined in a 2DEG.

In zinc-blende structures, the implicit bulk inversion asymmetry (BIA) induces a SO coupling in the electronic states of the material known as the Dresselhaus effect,[19] which is cubic in the electronic momentum **k**. If a confinement potential is applied to the structure so that a 2DEG is formed in the plane perpendicular to the confinement, the resulting bidimensional system also acquires a surface inversion asymmetry (SIA), which imposes another SO coupling in the structure known as the Rashba effect,[20] which is linear in **k**. Under this two-dimensional confinement, the BIA mechanism produces another contribution that is linear in **k**. Notice also that further lateral confinement to define the QD produces another **k**-linear SIA coupling, which affects the electronic structure of the system. We will show how these four possible SO terms are derived; two other possible terms vanish, as we will see.

In wide-gap QDs like GaAs, a unitary transformation[21–25] has been used in the full SO Hamiltonian. It yields, in a perturbative fashion,[26] only an effective diagonal SO term so that no state mixture—or level anticrossing (AC)—is observed in the QD spectrum. This approach is justifiable for wide-gap materials such as GaAs, since their SO couplings are small. However, in narrow-gap material QDs like InSb, where both BIA and SIA effects are stronger,[27] the treatment of the original full SO Hamiltonian is required. Here we consider a numerical diagonalization for both one- and two-particle QD problems. Among some of the few works that have dealt with narrow-gap nanostructures, Refs. 28–30, respectively, study spectroscopic properties, magneto-optical properties, and conduction band nonparabolicity effects of InSb QDs. Experiments in this material have explored the far-infrared response in lithographically defined dots,[30] as well as photoluminescence features in self-assembled dots.[31] However, Refs. 32 and 33, which deal with SO effects in the spectrum of InSb QDs, have a closer relationship with our work; the former takes into account both SIA terms due to the perpendicular and lateral confinements, where clear level ACs are visible in the spectrum, while the latter considers only the SIA term related to the lateral confinement, and no AC is observed in the spectrum.

We analyze in this work the role of each SO term in the definition of the electronic properties of narrow-gap QDs. For example, we will see which SO terms are able to induce ACs in the spectrum at given magnetic fields, where a strong and intrinsic (no phonon-assisted) spin mixing, and consequently intense SO-induced spin-flip relaxation processes are present. Other features related to ranges of critical magnetic fields, QD vertical and lateral sizes, *g*-factor, zero-field energy splittings and their possible cancellation by tuning SO terms, energy minigaps opened at the ACs, electron-electron interaction, and ground state singlet-triplet mixture for a two-

 

electron QD are also detailed. We find that the Rashba term is the one responsible for inducing level ACs, and the critical fields where they occur are shifted by the linear Dresselhaus term; the cubic BIA term becomes visible only at higher interfacial electric fields, when cancellation of linear BIA and SIA terms also occurs. For the two-electron problem, a singlet-triplet AC involving the QD ground state is observed, and the SO coupling is shown to act against (in favor of) the direct (exchange) Coulomb interaction.

The paper is organized as follows: Sec. II describes the theoretical approach embodying all the terms present in the full Hamiltonian; Sec. III explores the selection rules of each SO term, the critical field for the lowest energy (anti)crossing, and an important feature of the $g$-factor sign; Sec. IV shows the results for a one-electron QD, where an initial study is done separately for the influence of each SO term in the FD spectrum, and only then analysis of the simultaneous addition of all SO terms is done for different parameters defining the QD; Sec. V shows the results for a two-electron QD, where states are constructed by antisymmetrizing the FD basis, by looking at the competition between SO and electron-electron energies and also by discussing the mixture involving its ground state; at last, in Sec. VI we include our main conclusions.

## II. THEORETICAL METHOD

### A. Fock-Darwin spectrum

We assume the perpendicular confinement $V(z)$, which defines the 2DEG where the QD is built, to be strong enough so that the electronic states are completely localized in the first conduction subband of the system (a quantum well or a heterojunction); for example, in a triangular well, $V(z)=-eE_0z$, $E_0$ being the interfacial electric field. We consider also that the magnetic field is applied perpendicularly to the 2DEG plane, $\mathbf{B}=B_0(0,0,1)$. We assume further that the lateral confinement $V(\rho)$ defining the QD is parabolic; that is, $V(\rho)=m\omega_0^2\rho^2/2$, where $m$ ($\omega_0$) is the electronic effective mass (confinement frequency). In the absence of SO interactions, the Hamiltonian for the cylindrical QD so built is

$$H_0=\frac{\hbar^2}{2m}\mathbf{k}^2+\frac{m\omega_0^2}{2}\rho^2+\frac{g\mu_B}{2}\mathbf{B}\cdot\sigma, \tag{1}$$

where $\mathbf{k}=-i\nabla+e\mathbf{A}/(\hbar c)$, $\mathbf{A}=B_0\rho(-\sin\phi,\cos\phi,0)/2$ is the vector potential in the symmetric gauge, $\mu_B=e\hbar/(2m_0c)$ is the Bohr magneton, $g$ is the material bulk $g$-factor, and $\sigma$ stands for the Pauli matrices. The analytical solution of $H_0$ yields the well-known Fock-Darwin spectrum,[34–36]

$$E_{nl\sigma_Z}=(2n+|l|+1)\hbar\Omega+\frac{l}{2}\hbar\omega_c+g\mu_BB_0\frac{\sigma_Z}{2}, \tag{2}$$

where $\sigma_Z=\pm1$; $n=0,1,2,\ldots$ and $l=0,\pm1,\pm2,\ldots$ are, respectively, the radial and azimuthal quantum numbers; $\omega_c=eB_0/(mc)$ and $\Omega=\sqrt{\omega_0^2+\omega_c^2/4}$ are, respectively, the cyclotron and effective frequencies of the system, and the QD typical length scales are $l_0=\sqrt{\hbar/(m\omega_0)}$, $l_B=\sqrt{\hbar/(m\omega_c)}$, and $\lambda=\sqrt{\hbar/(m\Omega)}$, which refer, respectively, to the confinement, magnetic, and effective sizes of the system. The eigenfunctions of $H_0$ are given by

$$\Psi_{nl\sigma_Z}(x,\phi,\sigma_Z)=\frac{1}{\sqrt{2\pi}}R_{n|l|}(x)e^{il\phi}\chi_{\sigma_Z}, \tag{3}$$

where $x=\rho/\lambda$, $\chi_{\sigma_Z}$ is the spin eigenfunction, and the radial functions

$$R_{n|l|}(x)=\sqrt{\frac{2n!}{\lambda^2(n+|l|)!}}x^{|l|}e^{-x^2/2}L_n^{|l|}(x^2) \tag{4}$$

are given in terms of the associated Laguerre polynomials $L_n^{|l|}$.[37] It is interesting to rewrite $H_0$ in units of $\hbar\Omega$, as

$$\frac{H_0}{\hbar\Omega}=-\frac{1}{2x}\frac{\partial}{\partial x}\left(x\frac{\partial}{\partial x}\right)+\frac{L_Z^2}{2x^2}+\frac{x^2}{2}+\frac{\omega_c}{2\Omega}\left(L_Z+\frac{g\tilde{m}}{2}\sigma_Z\right), \tag{5}$$

where $\tilde{m}=m/m_0$ and $L_Z=-i\partial/\partial\phi$ is the $z$-orbital angular momentum.

### B. Rashba effect

Because of the surface inversion asymmetry originated from the perpendicular confinement defining the 2DEG, as well as the lateral confinement defining the QD, the SIA SO coupling must be added to $H_0$ for a correct description of the problem. Its usual Hamiltonian is

$$H_{SIA}=\alpha\sigma\cdot(\nabla V\times\mathbf{k}), \tag{6}$$

where $V(\mathbf{r})=V(\rho)+V(z)$ is the total confinement potential and $\alpha$ is the SO coupling parameter. After averaging over the quantized $z$ direction, this SO coupling can be decomposed as $H_{SIA}=H_R+H_{SIA}^D+H_K$, where

$$\frac{H_K}{\hbar\Omega}=i\frac{\alpha}{l_0^2}\frac{\omega_0}{\Omega}x\lambda\langle k_z\rangle(\sigma_+L_--\sigma_-L_+) \tag{7}$$

is zero because $\langle k_z\rangle=0$,

$$\frac{H_{SIA}^D}{\hbar\Omega}=\frac{\alpha}{l_0^2}\frac{\omega_0}{\Omega}\sigma_Z\left(L_Z+\frac{\omega_c}{\Omega}\frac{x^2}{2}\right) \tag{8}$$

is the spin-diagonal contribution due to the lateral confinement, and

$$\frac{H_R}{\hbar\Omega}=-\frac{1}{\hbar\Omega}\frac{\alpha}{\lambda}\frac{dV}{dz}[\sigma_+L_-A_-+\sigma_-L_+A_+] \tag{9}$$

is the well-known Rashba[20] term induced by the perpendicular confinement. In these equations, $L_\pm=e^{\pm i\phi}$, $\sigma_\pm=(\sigma_X\pm i\sigma_Y)/2$, and

$$A_\pm=\mp\frac{\partial}{\partial x}+\frac{L_Z}{x}+\frac{\omega_c}{2\Omega}x. \tag{10}$$

Notice that both nonzero terms are written in units of $\hbar\Omega$, are linear in $k$ and, in principle, are tunable: $H_{SIA}^D$ depends on the confinement frequency $\omega_0$, while $H_R$ depends on the interfacial field $dV/dz$ (in a triangular well, for example, $dV/dz=-eE_0$).

TABLE I. All of the terms present in the expression for the cubic Dresselhaus SO contribution, Eq. (16).

| Term | $i=1$ | $i=2$ | $i=3$ | $i=4$ |
|---|---|---|---|---|
| $A_{i1}$ | $-\frac{1}{4}$ | $-\frac{1}{4}$ | $\frac{1}{4}$ | $\frac{1}{4}$ |
| $A_{i2}$ | $\frac{3}{4}(1+L_Z)$ | $\frac{3}{4}(1-L_Z)$ | $\frac{1}{4}(1+L_Z)$ | $\frac{1}{4}(1-L_Z)$ |
| $A_{i3}$ | $-\frac{1}{4}(3+5L_Z+3L_Z^2)$ | $-\frac{1}{4}(3-5L_Z+3L_Z^2)$ | $-\frac{1}{4}(1+3L_Z+L_Z^2)$ | $-\frac{1}{4}(1-3L_Z+L_Z^2)$ |
| $A_{i4}$ | $\frac{1}{4}(8L_Z+4L_Z^2+L_Z^3)$ | $\frac{1}{4}(-8L_Z+4L_Z^2-L_Z^3)$ | $\frac{1}{4}(4L_Z^2-L_Z^3)$ | $\frac{1}{4}(4L_Z^2+L_Z^3)$ |
| $B_{i1}$ | $\frac{3}{8}$ | $-\frac{3}{8}$ | $\frac{1}{8}$ | $-\frac{1}{8}$ |
| $B_{i2}$ | $-\frac{3}{8}(1+2L_Z)$ | $-\frac{3}{8}(-1+2L_Z)$ | $-\frac{1}{8}(5+2L_Z)$ | $-\frac{1}{8}(-5+2L_Z)$ |
| $B_{i3}$ | $\frac{3}{8}(2L_Z+L_Z^2)$ | $\frac{3}{8}(2L_Z-L_Z^2)$ | $-\frac{3}{8}(2L_Z+L_Z^2)$ | $-\frac{3}{8}(2L_Z-L_Z^2)$ |
| $C_{i1}$ | $-\frac{3}{16}$ | $-\frac{3}{16}$ | $-\frac{1}{16}$ | $-\frac{1}{16}$ |
| $C_{i2}$ | $\frac{3}{16}L_Z$ | $-\frac{3}{16}L_Z$ | $-\frac{1}{16}(8+3L_Z)$ | $-\frac{1}{16}(8-3L_Z)$ |
| $D_{i1}$ | $\frac{1}{32}$ | $-\frac{1}{32}$ | $-\frac{1}{32}$ | $\frac{1}{32}$ |

It is interesting to mention that if the total Hamiltonian $H$ of the problem was only the sum of $H_0+H_{SIA}^D$, it would have an analytical solution.[33] Its spectrum would be the same as given in Eq. (2), with the substitution $\Omega$ by $\Omega_{\sigma_Z}=\sqrt{\omega_0^2+\omega_c^2/4+\sigma_Z(\alpha/l_0^2)\omega_0\omega_c}$, and the added contribution $\sigma_Z l(\alpha/l_0^2)\hbar\omega_0$ to that equation. Its radial functions would be the same as given in Eq. (4), with $\lambda$ substituted by $\lambda_{\sigma_Z}=\sqrt{\hbar/(m\Omega_{\sigma_Z})}$, changing also the $x$ variable to $\rho/\lambda_{\sigma_Z}$. The inclusion of $H_R$ makes $H$ a nondiagonal operator.

### C. Dresselhaus effect

If the QD is built in a zinc-blende crystalline structure material, its implicit lack of bulk inversion symmetry gives origin to the so-called Dresselhaus[19] SO coupling, or BIA term, which must also be added to $H_0$ in order to get an appropriate description of the system. The bulk BIA Hamiltonian is

$$H_{BIA}=\gamma[\sigma_X k_x(k_y^2-k_z^2)+\sigma_Y k_y(k_z^2-k_x^2)+\sigma_Z k_z(k_x^2-k_y^2)], \tag{11}$$

where $\gamma$ is the SO coupling parameter. After the $z$ quantization defining the 2DEG in the $xy$ plane, $H_{BIA}$ can be separated as $H_{BIA}=H_D^L+H_D^Q+H_D^C$, where $H_D^L=\gamma\langle k_z^2\rangle[\sigma_Y k_y-\sigma_X k_x]$ is linear in $k$, $H_D^Q=\gamma\sigma_Z\langle k_z\rangle(k_x^2-k_y^2)$ is quadratic in $k$, and $H_D^C=\gamma[\sigma_X k_x k_y^2-\sigma_Y k_y k_x^2]$ is cubic in $k$. One can notice that the quadratic (spin diagonal) term can be written as

$$\frac{H_D^Q}{\hbar\Omega}=\frac{1}{\hbar\Omega}\frac{\gamma\langle k_z\rangle}{\lambda^2}\sigma_Z[L_+^2B_+ + L_-^2B_-], \tag{12}$$

where we have defined

$$B_\pm=\left(-\frac{\partial}{\partial x}+\frac{1\pm 2L_Z}{x}\pm\frac{\omega_c}{\Omega}x\right)\frac{1}{2}\frac{\partial}{\partial x} -\left(\frac{\pm 2+L_Z}{x^2}+\frac{\omega_c}{\Omega}\right)\frac{L_Z}{2}-\frac{\omega_c^2}{8\Omega^2}x^2. \tag{13}$$

This term corresponds to a mass renormalization in the 2DEG plane, which would then become spin dependent and would be different in $x$ and $y$ directions; however, such a term vanishes since $\langle k_z\rangle=0$. The linear contribution can be written as

$$\frac{H_D^L}{\hbar\Omega}=-\frac{i}{\hbar\Omega}\frac{\gamma\langle k_z^2\rangle}{\lambda}[\sigma_+L_+A_+-\sigma_-L_-A_-], \tag{14}$$

where $\langle k_z^2\rangle=(\pi/z_0)^2$ if an infinite well defines the 2DEG, $z_0$ being the typical length scale in the $z$ direction. As for the cubic contribution, after some algebra,[38,39] it can be expressed as

$$\frac{H_D^C}{\hbar\Omega}=\frac{i}{\hbar\Omega}\frac{\gamma}{\lambda^3}\left\{\sigma_-L_+^3\left[A_1+\frac{\omega_c}{\Omega}B_1+\frac{\omega_c^2}{\Omega^2}C_1+\frac{\omega_c^3}{\Omega^3}D_1\right] +\sigma_+L_-^3\left[A_2+\frac{\omega_c}{\Omega}B_2+\frac{\omega_c^2}{\Omega^2}C_2+\frac{\omega_c^3}{\Omega^3}D_2\right] +\sigma_-L_-\left[A_3+\frac{\omega_c}{\Omega}B_3+\frac{\omega_c^2}{\Omega^2}C_3+\frac{\omega_c^3}{\Omega^3}D_3\right] +\sigma_+L_+\left[A_4+\frac{\omega_c}{\Omega}B_4+\frac{\omega_c^2}{\Omega^2}C_4+\frac{\omega_c^3}{\Omega^3}D_4\right]\right\}, \tag{15}$$

where the abbreviations

$$A_i=A_{i1}\frac{\partial^3}{\partial x^3}+A_{i2}\frac{1}{x}\frac{\partial^2}{\partial x^2}+A_{i3}\frac{1}{x^2}\frac{\partial}{\partial x}+A_{i4}\frac{1}{x^3},$$

$$B_i=B_{i1}x\frac{\partial^2}{\partial x^2}+B_{i2}\frac{\partial}{\partial x}+B_{i3}\frac{1}{x},$$

$$C_i=C_{i1}x^2\frac{\partial}{\partial x}+C_{i2}x,$$

$$D_i=D_{i1}x^3, \tag{16}$$

with $i=1,2,3,4$, are introduced, and are given in Table I.

One must point out that in a magnetic field the matrix elements of $H_D^C$ are not Hermitian, so that the usual symmetrization procedure is required;[13,40] at zero field, such a problem does not occur.[18] Notice that also $H_D^L$ can, in principle, be varied by changing the size $z_0$, and that both nonzero BIA terms are written in units of $\hbar\Omega$.[41]

### D. Electron-electron interaction and total Hamiltonian

For the inclusion of the Coulomb interaction in the QD, we expand the quantity $|\mathbf{r}_1-\mathbf{r}_2|^{-1}$ in the Hamiltonian $H_{ee}=e^2/(\varepsilon|\mathbf{r}_1-\mathbf{r}_2|)$ in terms of Bessel functions[37] $J_p$; this yields, in units of $\hbar\Omega$,

$$\frac{H_{ee}}{\hbar\Omega}=\frac{\lambda}{a_B}\sum_{p=-\infty}^{\infty}e^{ip(\phi_1-\phi_2)}\int_0^{\infty}d\xi J_p(\xi x_1)J_p(\xi x_2)e^{-\xi z_0/\lambda}, \quad (17)$$

where $\varepsilon$ is the material dielectric constant and $a_B=\varepsilon\hbar^2/(me^2)$ is the effective Bohr radius in the material. The two-particle states are properly antisymmetrized in the construction of Slater determinants based on the one-particle functions of Eq. (3), so that both direct and exchange Coulomb contributions are included; such states may be labeled by the projections of the orbital ($M_L$) and spin ($M_S$) total angular momenta. Even though the $p$-sum in Eq. (17) is infinite, in practice, when one makes the angular integration of an element like $\langle M_L M_S|H_{ee}|M_L' M_S'\rangle$, which involves calculations of $\langle\Psi_i(1)\Psi_j(2)|H_{ee}|\Psi_k(1)\Psi_l(2)\rangle$, one has only one nonzero $p$ contribution obeying $\delta_{l_i+l_j,l_k+l_l}$. Therefore, the Coulomb matrix elements must satisfy $\delta_{M_L,M_L'}$ as expected,[42] and certainly they also satisfy $\delta_{M_S,M_S'}$, since the Coulomb interaction is not spin dependent.

After separately exposing Eqs. (5), (8), (9), (14), (15), and (17), all Hamiltonians must be taken into account in the full diagonalization of the system, so that the QD total one-particle Hamiltonian $H$ is given by

$$H=H_0+H_{SIA}^D+H_R+H_D^L+H_D^C; \quad (18)$$

when an interacting two-particle QD is studied, its total Hamiltonian $\widetilde{H}$ will then be given by

$$\widetilde{H}=\sum_{i=1}^{2}H+H_{ee}. \quad (19)$$

## III. SELECTION RULES, CRITICAL FIELD, AND $g$-FACTOR SIGN

Before showing spectra of parabolic QDs under the influence of SO coupling, the way in which Eqs. (5), (8), (9), (14), (15), and (17) were written allows us to anticipate some general features of the SO influence on the system. The selection rules describe which levels will cross or anticross at a given magnetic field. Notice immediately that $H_{SIA}^D$, $H_R$, and $H_D^L$ have only linear dependence on the magnetic field $B_0$, while $H_D^C$ has linear, quadratic, and cubic contributions on $B_0$.

The various Hamiltonian terms yield explicit selection rules dictating which levels $\{n,l,\sigma_Z\}$ of $H_0$ will be influenced by the distinct SO effects. At zero field and due to the $\sigma_Z L_Z$ term, $H_{SIA}^D$ splits the FD spectrum according to the total $z$-angular momentum, $j=l+\sigma_Z/2$. At a finite field, $H_R$ induces a set of ACs in the FD spectrum whenever $\Delta l=\pm 1=-\Delta\sigma_Z/2$; due to the $\sigma_\pm L_\mp$ terms, mostly negative $l$'s are affected since their magnetic dispersions allow for crossings, and the lowest AC occurs between the levels $\{0,0,-1\}$ and $\{0,-1,+1\}$ at a given critical field $B_C$. In addition, at a finite field and via the $\sigma_\mp L_\pm^3$ terms, $H_D^C$ is able to induce sets of ACs in levels where $\Delta l=\mp 3$ and $\Delta\sigma_Z/2=\pm 1$, the first (second) one at low energies involving the levels: $\{0,1,-1\}$ and $\{0,-2,+1\}$ ($\{0,0,-1\}$ and $\{0,-3,+1\}$). The terms $\sigma_\pm L_\pm$ in both $H_D^L$ and $H_D^C$ do not induce ACs at low energies, but rather split and shift the FD spectrum due to matrix elements where $\Delta l=\pm 1=\Delta\sigma_Z/2$. Notice that matrix elements between states with different $n$'s are in general nonzero, so that the full diagonalization involves mixings with various $n$ values.

The pure $H_0$ spectrum at zero field has three lowest energy shells that contain, in increasing energy, the states: $\{0,0,\pm 1\}$; $\{0,-1,\pm 1\}$ and $\{0,1,\pm 1\}$; $\{0,-2,\pm 1\}$, $\{1,0,\pm 1\}$, and $\{0,2,\pm 1\}$. Inclusion of SO couplings produces the first shell to have $j=1/2$, while the second (third) shell is subdivided in $j=1/2$ and $3/2$ ($j=1/2$, $3/2$, and $5/2$). A finite magnetic field lifts orbital and spin degeneracies of the states (so that levels with negative $l$ and positive $\sigma_Z$ acquire lower energies in a QD having a negative $g$-factor) and introduces a competition between external magnetic field and SO effects in the one-electron QD spectrum. In the two-electron case, such competition also involves both direct and exchange Coulomb interactions.

Because $g<0$ in an InSb QD, its ground state has $l=0$ and $\sigma_Z=+1$, while the lowest energy crossing of $H_0$, related to the states $\{0,0,-1\}$ and $\{0,-1,+1\}$, occurs at a critical magnetic field given by $E_{00-1}=E_{0-1+1}$, which yields

$$B_C^0=\frac{\hbar\omega_0}{\mu_B}\frac{\widetilde{m}}{\sqrt{\widetilde{m}|g|(\widetilde{m}|g|+2)}}. \quad (20)$$

Notice that $B_C^0$ may be decreased by reducing the QD confinement energy. Its moderate value in InSb (which we anticipate to be around 2.5 T for $\hbar\omega_0=15$ meV) is a direct consequence of its high $g$-factor; on the other hand, in a GaAs QD, even in a weak confinement ($\hbar\omega_0=2$ meV), we have $B_C^0\simeq 9.5$ T, a field where the Landau levels are already well defined. As already discussed, the inclusion of $H_R$ transforms such crossing into an AC, opening an energy gap at $B_C\simeq B_C^0$; we will see below how the linear BIA term is able to shift such a field to higher values.

There is an interesting feature related to the influence of the $g$-factor sign on the QD spectrum. We have just mentioned that in a $g<0$ QD, $H_R$ induces ACs in the low-energy FD spectrum while $H_D^L$ shifts them to higher fields. On the other hand, in a $g>0$ QD, the level sequence is permuted and consequently the roles of $H_D^L$ and $H_R$ are interchanged; to visualize such a fact, it is enough to verify that the ground state turns to have $l=0$ and $\sigma_Z=-1$, while the lowest FD crossing is between the states $\{0,0,+1\}$ and $\{0,-1,-1\}$, and to remember out the form of the operators in Eqs. (9) and (14). Notice that in a silicon QD (being a non-zinc-blende material having positive $g$), for example, the BIA Hamiltonian is absent while the SIA term is not able to induce those ACs in the spectrum.

Regarding $H_{ee}$, at zero field the Coulomb interaction is able to split the spectrum in singlets and triplets. A magnetic field may alter the sequence of levels; for example, the QD

TABLE II. Parameters for the InSb QD used in our calculations, if no other numbers are specified. See text for definitions of different quantities.

| $E_H$ (meV) | $dV/dz$ (meV Å$^{-1}$) | $\gamma$ (eV Å$^3$) | $a_B$ (Å) | $\alpha$ (Å) | $\varepsilon$ | $\tilde{m}$ | $g$ |
|---|---|---|---|---|---|---|---|
| 23 | −0.5 | 160 | 625 | 500 | 16.5 | 0.014 | −51 |
| $\hbar\omega_0$ (meV) | $E_{SIA}^D$ (meV) | $E_R$ (meV) | $E_D^C$ (meV) | $E_D^L$ (meV) | $E_{ee}$ (meV) | $l_0$ (Å) | $z_0$ (Å) |
| 15 | 0.2 | 1.3 | 0.02 | 5.2 | 4.5 | 190 | 40 |

ground state may oscillate between singlet and triplet states as the field is increased. Inclusion of SO couplings is able to mix such states at different critical fields and to induce intrinsic (non-phonon-assisted) mixing involving the QD ground state, as we will see below.

## IV. RESULTS FOR ONE-ELECTRON QDS

It is important to emphasize that the perturbative approach used in GaAs QDs is not valid in narrow-gap materials, which are the focus of this work, so that an exact diagonalization of the full Hamiltonian becomes necessary. For a better understanding of the one-particle full spectrum of $H$ as a function of $B_0$ in an InSb QD, we will progressively discuss the changes in the FD spectrum of $H_0$ as induced by each of the four possible SO terms; next, we consider all SO terms simultaneously. In the numerical diagonalization we consider all states in the FD basis having $n \leqslant 4$ and $|l| \leqslant 9$, which is equivalent to the first ten energy shells at zero field and embodies a basis of 110 states. The defining parameters of the QD are given in Table II if no other numbers are specified. The SO and Coulomb energies are taken from their respective prefactors, that is, $E_{SIA}^D = (\alpha/l_0^2)\hbar\omega_0$, $E_R = (\alpha/\lambda)dV/dz$, $E_D^L = \gamma\langle k_z^2\rangle/\lambda$, $E_D^C = \gamma/\lambda^3$, and $E_{ee} = (\lambda/a_B)\hbar\Omega$; the $\alpha$ and $\gamma$ values are the ones of Ref. 33, although they cannot be taken as unique: for example, Ref. 27 yields $\gamma = 220$ eV Å$^3$. Certainly, such typical energies vary for different levels, and change with magnetic field and QD material, although they provide a measure of the relative importance of various Hamiltonians terms; notice that $E_D^L$ is comparable to $E_{ee}$ and that $E_R$ can be made equal to $E_D^L$ by quadruplicating $dV/dz$.

To avoid repetition in the following, one should keep in mind that the next 10 figures—from Fig. 1 to Fig. 10—have the same structure: panels A show QD spectra for the full FD basis (110 states); panels B show a zoom of the three lowest energy shells, with insets showing another zoom of the four levels of the second energy shell; panels C and D show, respectively, the $B_0$ evolution of the expectation values of the spin operator $\langle\Upsilon|\sigma_Z|\Upsilon\rangle = \langle s_Z\rangle$ and of the corresponding angular momentum $\langle\Upsilon|L_Z|\Upsilon\rangle = \langle l_Z\rangle$ for each state $|\Upsilon\rangle$ obtained after diagonalization of $H$ for the full FD basis, while their insets do the same, but only for the seven lowest energy levels. Parameters of Table II are used from Fig. 1 to Fig. 8, while Fig. 9 (Fig. 10) considers a doubled $z_0$ size (a four times stronger $dV/dz$ field). One has to keep in mind that, when referring to state labels in this work, the FD quantum numbers will be used even when SO coupling is present,

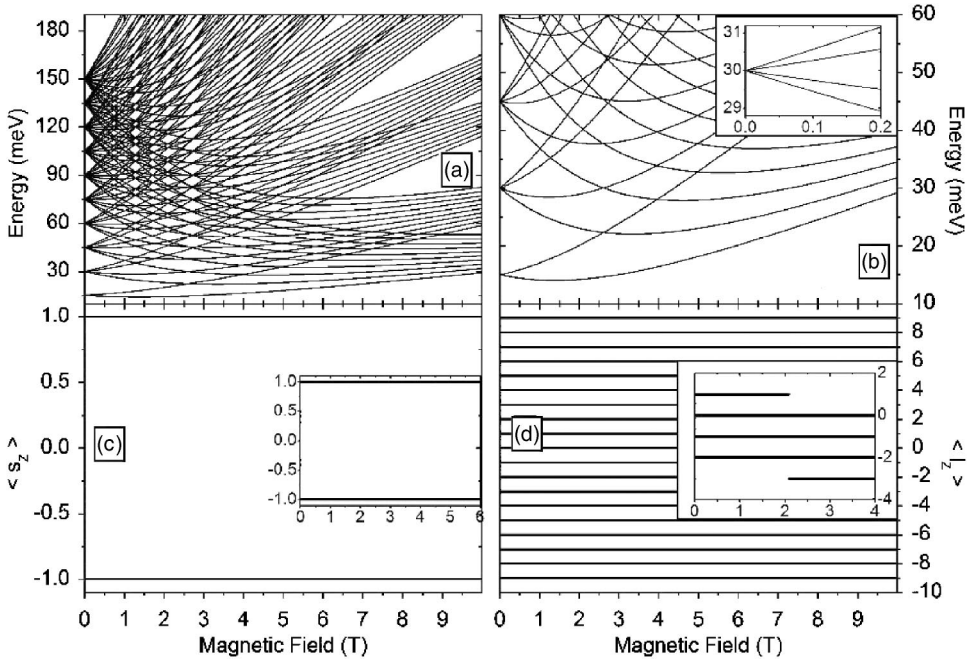


FIG. 1. $H_0$ FD spectrum of an InSb QD as defined by parameters in Table II (no SO terms). Notice the energy shell structure at zero magnetic field, and the presence of several accidental degeneracies at finite fields. The states are *pure*, since the expectation values of spin and orbital angular momenta are only integer numbers at any field.

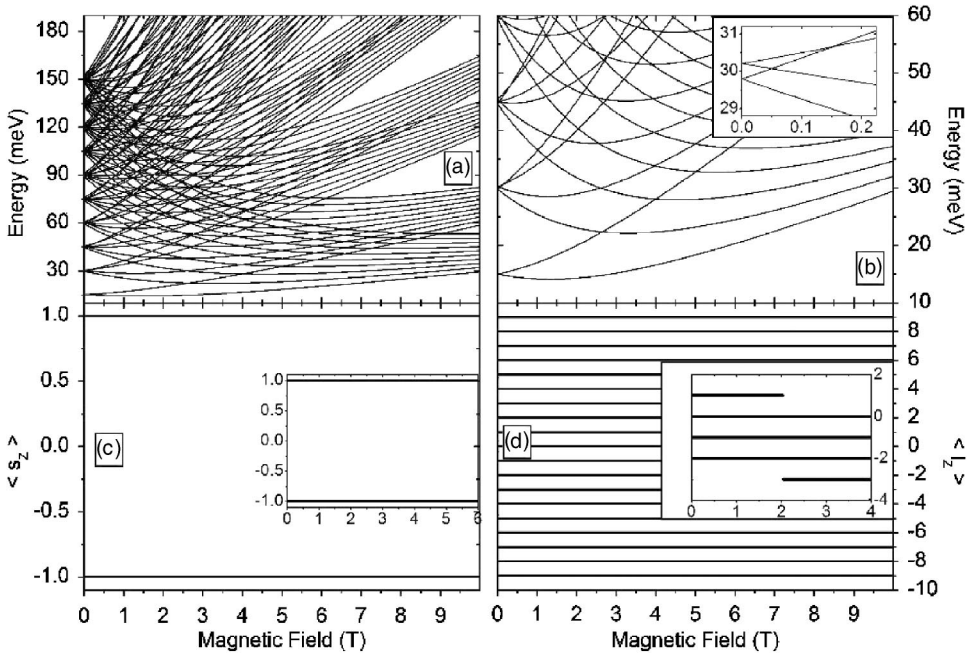


FIG. 2. QD spectrum when only the diagonal SIA term $H_{SIA}^{D}$ is added to $H_0$. States continue to be pure at any field, and new accidental degeneracies are induced in the low-field spectrum as exemplified in inset of panel B; this introduces a competition between SO and magnetic field effects in QD electronic properties.

where then the FD levels are certainly no longer pure.

As a starting and reference point, we show in Fig. 1 the pure $H_0$ spectrum, with no SO effects. The main features in panel A are the zero-field QD energy shell structure (with separation of 15 meV between successive shells), the lifting of spin and orbital degeneracies by a finite field, the presence of accidental degeneracies at specific magnetic fields, the larger $B_0$ dispersion of the $l>0$ orbitals, and the formation of well defined Landau levels at high fields. It is easier to see in panel B the level sequence for the first three shells mentioned before; for example, at $B_0=0.5$ T, before any accidental degeneracy point, the twelve lowest states, in increasing energy, are $\{0,0,+1\}$, $\{0,0,-1\}$, $\{0,-1,+1\}$, $\{0,-1,-1\}$, $\{0,1,+1\}$, $\{0,1,-1\}$, $\{0,-2,+1\}$, $\{0,-2,-1\}$, $\{1,0,+1\}$, $\{1,0,-1\}$, $\{0,2,+1\}$, and $\{0,2,-1\}$. Notice also that $B_C^0 \simeq 2.6$ T gives the lowest energy crossing. In the inset of this panel we show that the second shell, away from accidental degeneracy points, presents no further level crossing in the FD spectrum. Panels C and D and their insets confirm that no level mixture is present in the $H_0$ spectrum, since every state takes only integer values: $\langle s_Z\rangle = \pm 1$ and $-9<\langle l_Z\rangle<9$. All of these general features are clear signatures of parabolic QDs.

### A. Influence of SIA terms

The addition of the diagonal SIA term $H_{SIA}^{D}$ to $H_0$, shown in Fig. 2, causes small splittings in the zero-field spectrum, but it is not able to shift the accidental degeneracy points present at finite fields (panel A), so that the critical field $B_C$ where the first level crossing occurs is not altered by $H_{SIA}^{D}$, and then one has $B_C \simeq B_C^0 \simeq 2.6$ T (panel B). The splittings, however, induce new level crossings at low fields, as exemplified in the inset of panel B for the second shell; this result is due to the fact that $H_{SIA}^{D}$ orders states according to their $j$ value, and the highest (lowest) zero-field energy level has $j=3/2$ ($j=1/2$) in this shell, where it can be noticed that for $B_0 \gtrsim 0.2$ T the "normal" ordering of states (existent in the absence of SO terms) for $g<0$ is restored: $\{0,-1,+1\}$, $\{0,-1,-1\}$, $\{0,1,+1\}$, $\{0,1,-1\}$ in increasing energy (also notice that both $j=3/2$ and $j=1/2$ states are equidistant from the pure $H_0$ value of 30 meV at $B_0=0$). This competition between SO and magnetic field effects is identical to the Zeeman and Paschen-Back regimes of real atoms;[43] the same level ordering is observed in Ref. 33, where the SIA term $H_R$ is not taken into account. Panels C and D and their insets confirm that this diagonal SO Hamiltonian does not introduce any level mixture in the FD states, and so the QD levels continue to be pure even under $H_{SIA}^{D}$ effects.

The addition of the Rashba SIA term $H_R$ to $H_0$, shown in Fig. 3, introduces a strong state mixture, whatever be the magnitude of $\alpha$, whenever a pair of FD levels satisfying $\Delta l = -\Delta\sigma_Z/2 = \pm 1$ cross in a given accidental degeneracy of the $H_0$ spectrum (panel A). This mixture converts the crossing in $B_C^0$ into an AC and opens an energy gap at a slightly shifted critical field $B_C \simeq 2.5$ T $\lesssim B_C^0$ (panel B). Panels C and D and their insets show that higher energy levels also satisfying that selection rule exhibit ACs approximately at this same $B_C$ value, giving origin to the "$\chi$" collapse seen in both $\langle s_Z\rangle$ and $\langle l_Z\rangle$ values around 2.5 T; the range of critical fields (between 2.1 and 2.6 T), as well as the size of the energy gaps opened at those ACs, are proportional to the magnitude of $\alpha$, such that $B_C$ decreases upon increasing $\alpha$. $H_R$ also induces small splittings in the zero-field spectrum and slightly shifts accidental degeneracy points at finite fields. Notice in the inset of panel B that the zero-field level sequence in the second shell is opposite to the previous figure, that is, $j=1/2$ ($j=3/2$) state has the highest (lowest) energy, and the $j=1/2$ state has practically the same value as for $H_0$; for $B_0 \gtrsim 0.1$ T, the normal ordering of states is restored. Notice in panel D that every originally negative even $l$ state ($l=-2,-4,-6,-8$) anticrosses, while only some of the states having an original negative odd value of $l$ also anticross.

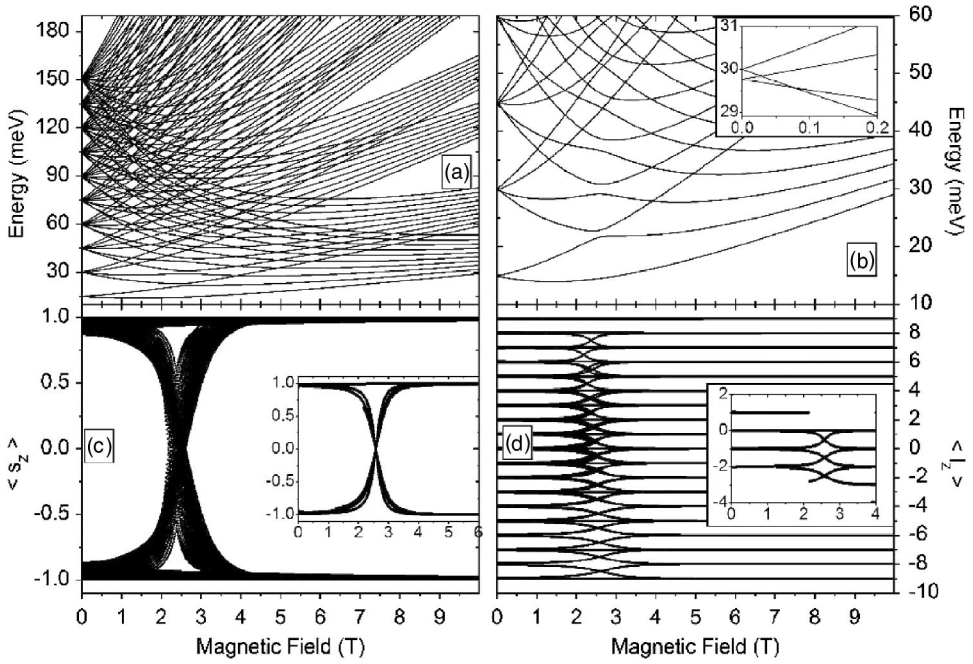


FIG. 3. QD spectrum when only the Rashba SIA term $H_R$ is added to $H_0$. Strong level mixtures occur at $B_C \simeq 2.5$ T for all states satisfying the selection rules, causing the observed ACs (panels C and D). Notice the inverted level crossing in inset of panel B when compared to Fig. 2.

Figure 4 shows the simultaneous addition of both SIA terms, $H_{SIA}^D$ and $H_R$, to $H_0$. Observe in the inset of panel B that the ordering of states is the one derived from $H_{SIA}^D$, however, their energies ($j=3/2$ at 30 meV and $j=1/2$ at a slightly smaller value), as well as the field ($B_0 \gtrsim 0.1$ T) where the normal state ordering is restored, are determined by $H_R$. The range of critical fields is wider (between 2.2 and 3.6 T in panel C), and one can see in panel D that orbitals having $\langle l_Z \rangle < 0 (\langle l_Z \rangle > 0)$ present ACs at fields smaller (greater) than the field $B_C \simeq 2.55$ T of the first AC (shown in insets of panels C and D). For future comparison, notice in panel B that the first AC involving $n=1$ states ($\simeq 50$ meV, related to $\{0,1,-1\}$ and $\{1,0,+1\}$ levels) occurs at that same $B_C$ value; in general, ACs between states with any $n$ value happen inside the same range of critical fields, which is clear in panels C and D. It is important to remember that both SIA influences can be reduced by decreasing $\omega_0$ (in $H_{SIA}^D$) or $dV/dz$ (in $H_R$).

### B. Influence of BIA terms

The addition of the cubic Dresselhaus term $H_D^C$ to $H_0$ (Fig. 5) has practically no effect on the pure $H_0$ spectrum, as seen in panels *A* and *B*. In panels C and D, small state mixtures are visible at $B_0 \simeq 1$ T and $B_0 \simeq 5$ T, both involving ACs satisfying $\Delta l = \mp 3$ and $\Delta \sigma_Z / 2 = \pm 1$; the first AC at 1 T (5 T) is between states $\{0,1,-1\}$ and $\{0,-2,+1\}$ ($\{0,0,-1\}$ and $\{0,-3,+1\}$). $H_D^C$ is also able to induce zero-field splittings in

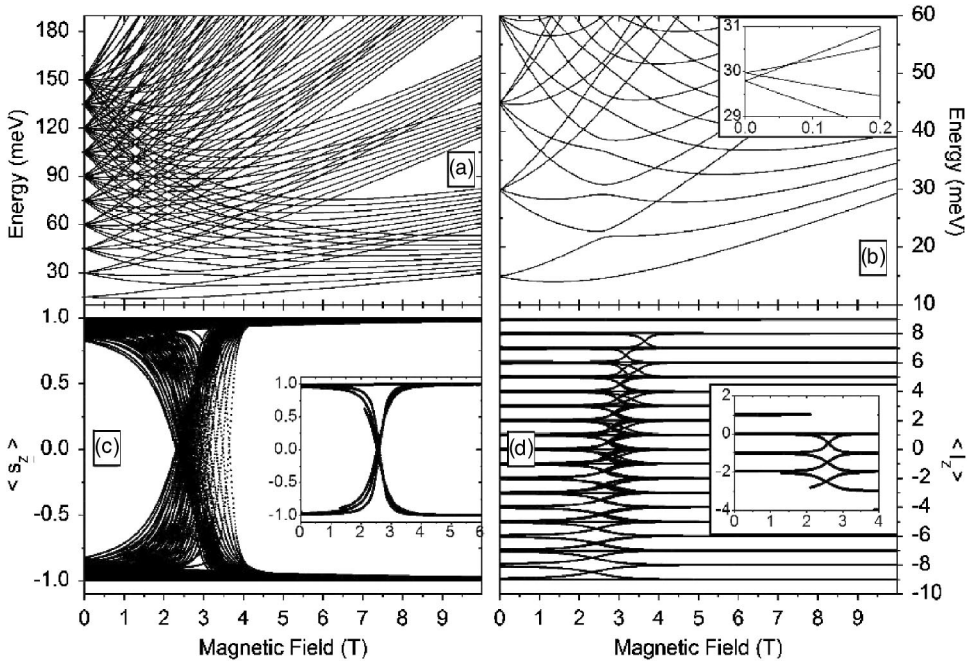


FIG. 4. QD spectrum when both SIA terms, $H_{SIA}^D$ and $H_R$, are added to $H_0$. The critical field range for ACs becomes wider (panels C and D), even though the first AC happens practically at the same field of the previous figure ($B_C \simeq 2.55$ T in insets of those panels). Anticrossings involving $l<0$ ($l>0$) orbitals are shifted to lower (higher) fields as seen on panel D.

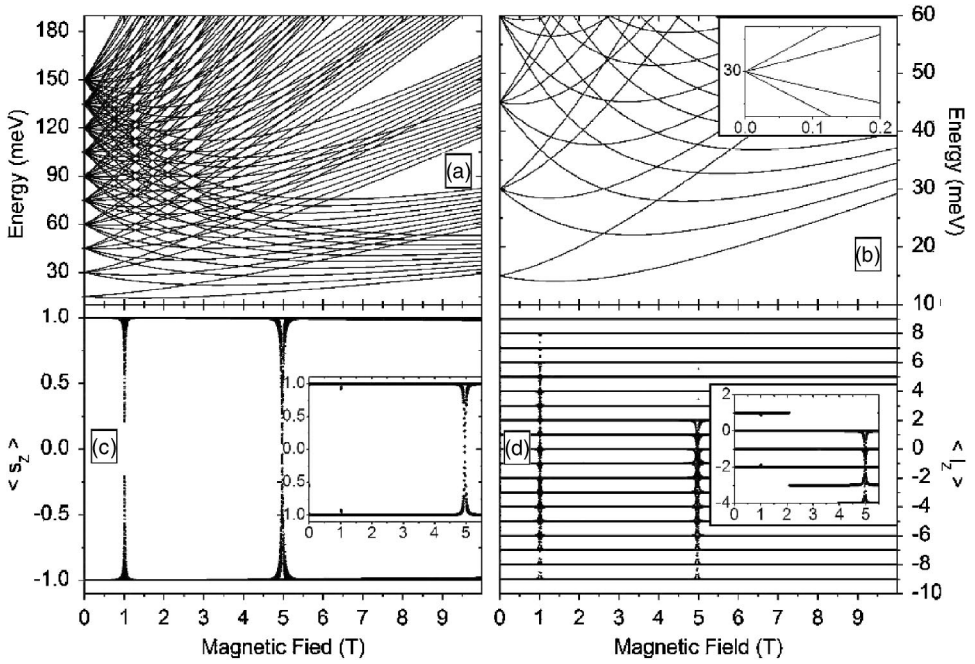


FIG. 5. QD spectrum when only the cubic BIA term $H_D^C$ is added to $H_0$. The influence of such term on the QD electronic properties is practically negligible for the parameters of Table II; it will be important for the full $H$ when we later consider the Rashba effect.

the FD spectrum due to matrix elements where $\Delta l = \pm 1 = \Delta\sigma_Z/2$; however, such splittings and gaps opened at the ACs are negligible because of the weak influence of this cubic term when it is considered separately from the other SO terms. Its influence will be more important when we later consider the full $H$ for the QD.

The addition of the linear Dresselhaus term $H_D^L$ to $H_0$ (Fig. 6) drastically changes the general features of the FD spectrum, inducing strong zero-field splittings and shifting the accidental degeneracies to higher fields (panels A and B). The respective matrix elements ($\Delta l = \pm 1 = \Delta\sigma_Z/2$) are not able to introduce low energy ACs in the system, as seen on insets of panels C and D (the ACs visible around 8.5 T on these panels are related to higher energy levels). As seen on Panels A and B, the zero-field splittings are so strong that QD states cease to be pure *even at zero field*, as shown in panels C and D. As an example, notice in panel C that at $B_0 = 0$, values of $|\langle s_Z \rangle| \simeq 0$ are found for higher energy states, while in its inset, related only to the seven lowest energy levels, one finds values of $|\langle s_Z \rangle| \simeq 0.5$. As an example of the

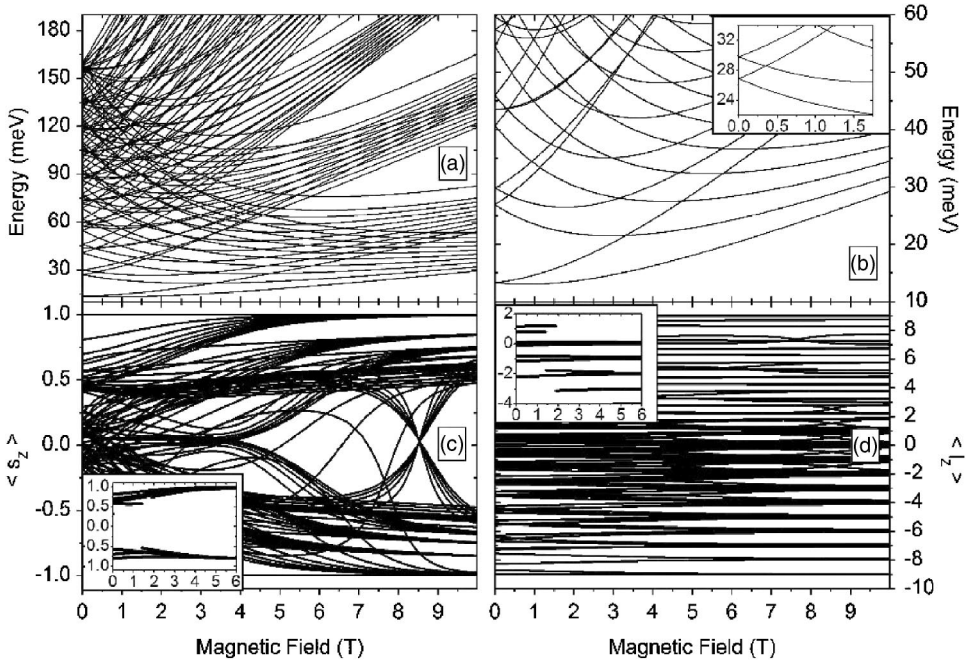


FIG. 6. QD spectrum when only the linear BIA term $H_D^L$ is added to $H_0$. $H_D^L$ is not able to induce low energy ACs. However, it drastically alters the spectrum by introducing enormous zero-field splittings and large shifts of several crossings at finite fields (panels A and B); for example, the first crossing has moved to about 3.3 T. Even the lowest energy states cease to be pure at low fields (insets of panels C and D). Notice only one crossing of the second shell levels in inset of panel B, instead of two as in previous figures.

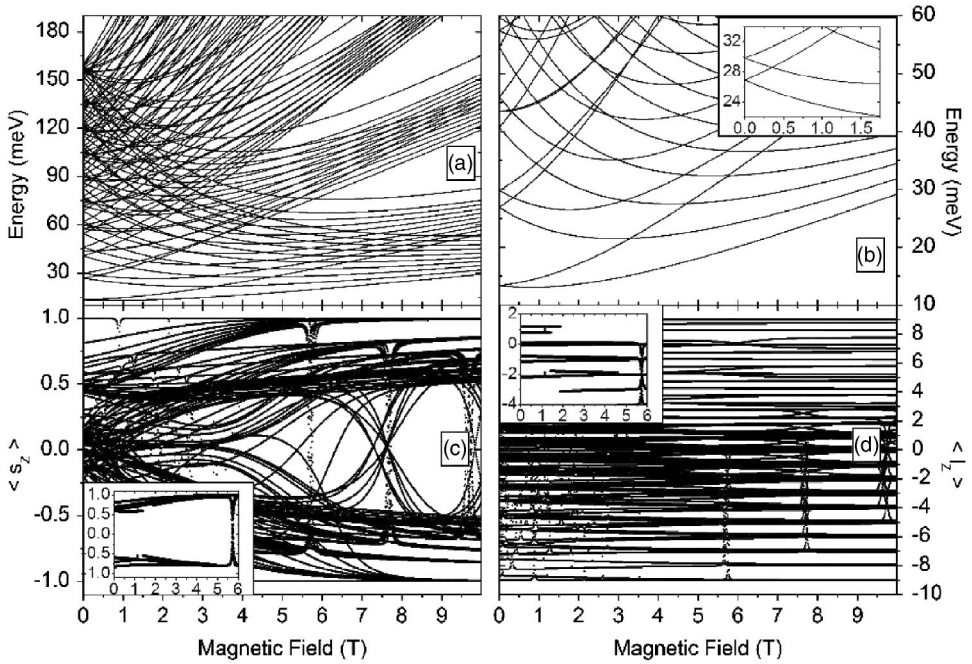


FIG. 7. QD spectrum when both BIA terms, $H_D^C$ and $H_D^L$, are added to $H_0$. Under the parameters of Table II, the linear Dresselhaus contribution dominates over the cubic one. The strong mixings at low fields are due to $H_D^L$, while the low energy ACs are due to $H_D^C$.

shifting of the level crossings to higher fields, observe that the first one occurs at $B_C \simeq 3.3$ T (remember that $B_C^0 \simeq 2.6$ T). Other essential feature of $H_D^L$ is shown in inset of panel B: only one crossing is present in the second shell (at about 0.45 T), the second one occurring only at a field around 3.5 T, so that the normal state ordering is no longer restored with field. This makes impossible the identification of distinct Zeeman and Paschen-Back regimes in the QD spectrum as has been happening with the previous SO terms. $H_D^L$ is responsible for most of the QD states being no longer pure at *any* field, a point which will be essential later in the discussion of the full Hamiltonian spectrum. As a note, in that same panel B inset, the highest (lowest) energy state at zero field has $j=3/2$ at 30 meV, the same energy of the pure $H_0$ ($j=1/2$ at around 27 meV). Remember also that the influence of $H_D^L$ in the spectrum can be decreased by increasing the well size $z_0$.

Figure 7 shows the simultaneous addition of both BIA terms, $H_D^C$ and $H_D^L$, to $H_0$. It is visible on panels A and B, as expected from the last paragraphs, that the linear contribution dominates over the cubic one in the overall features of the QD spectrum and in the strong mixing of levels. For low energy states, notice in insets of panels C and D the strong mixing at low fields (due to $H_D^L$) and the AC (due to $H_D^C$) shifted to 5.7 T (from 5 T in Fig. 5). We emphasize, however, that the influence of the cubic term will be larger when we later consider nonzero Rashba fields.

### C. Influence of all SO terms

Figure 8 finally shows the QD spectrum when all SO terms are simultaneously taken into account; that is, the one-particle full $H$ spectrum from Eq. (18). From the previous isolated term discussions, one may identify which SO mechanisms are dominant in each of the main features of the spectrum. An enormous state mixture even at magnetic fields close to zero (panels C and D and their insets), as well as splitting, position, and ordering of states (panels A and B) are dominated by $H_D^L$, although with contributions from the SIA terms. From the two sets of low energy ACs (insets in panels C and D), the one around $B_C \simeq 3.3$ T is due to the $H_R$ selection rules, while the other around 5.7 T is due to $H_D^C$. These ACs are shifted by $\simeq 0.7$ T to a higher field because of the influence of $H_D^L$: remember that in Fig. 4 we had $B_C \simeq 2.55$ T, while in Fig. 5 the respective AC happened at 5 T. High energy ACs inside those sets (mainly at 3.3 T) have their respective magnetic fields slightly decreased due to $H_{SIA}^D$. The distinct feature of the full $H$ spectrum is the clear presence of more than one value of critical fields where ACs occur. By comparing panels A and C, and considering mainly the ACs originated from the Rashba term (as those gaps are the largest), one notes that the first family of ACs (around 3.3 T, related to states between 20 and 70 meV) involves only $n=0$ levels, occurring between pairs such as $\{0,0,-1\}$ and $\{0,-1,+1\}$, $\{0,-1,-1\}$ and $\{0,-2,+1\}$, $\{0,-2,-1\}$ and $\{0,-3,+1\}$, etc. The second family of ACs (around 5 T, related to states between 70 and 120 meV) involves only $n=1$ levels (except the first one), involving states $\{0,1,-1\}$ and $\{1,0,+1\}$, $\{1,0,-1\}$ and $\{1,-1,+1\}$, $\{1,-1,-1\}$ and $\{1,-2,+1\}$, etc. The third family of ACs (around 8 T, related to states between 130 and 180 meV) involves only $n=2$ levels (except the first and second), involving states $\{0,2,-1\}$ and $\{1,1,+1\}$, $\{1,1,-1\}$ and $\{2,0,+1\}$, $\{2,0,-1\}$ and $\{2,-1,+1\}$, etc. Although the main ACs in the QD spectrum are caused by the $H_R$ mixtures, one can conclude that the presence of $H_D^L$ in the full $H$ dislocates them in such a way as to group ACs related to a same $n$ value around the same critical field. The reason for that can be understood by comparing panels B and their insets in Figs. 4 and 6. In the former, there are two crossings at low fields in the second shell, so that the rearrangement of levels produces the first AC involving an $n=1$ level (between $\{0,1,-1\}$ and $\{1,0,+1\}$ around

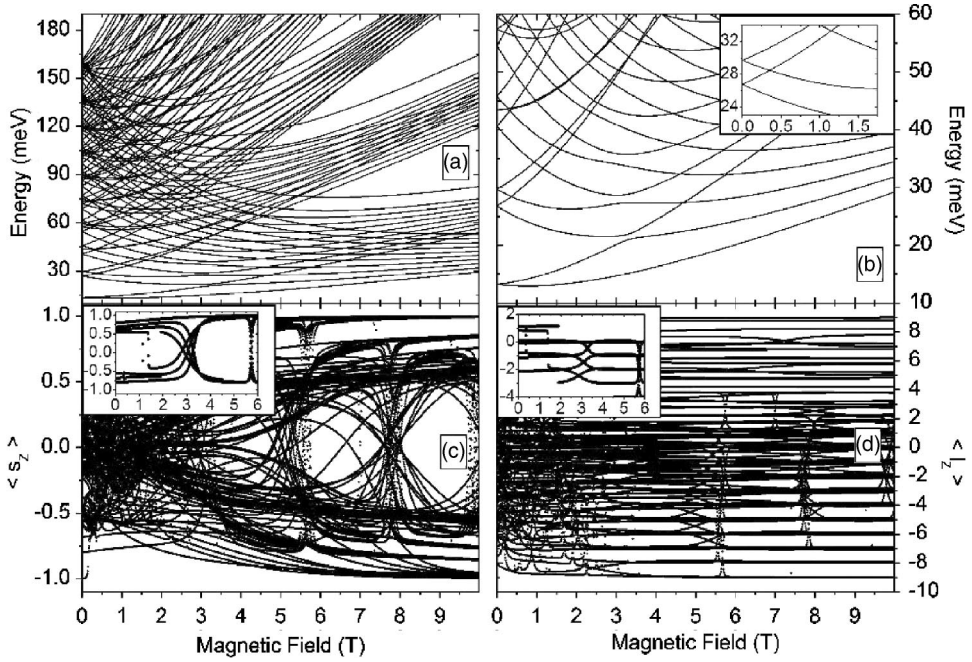


FIG. 8. One-particle full $H$ spectrum of an InSb QD as defined by parameters in Table II (all SO terms simultaneously added to $H_0$). Basically, $H_R$ induces the main low energy ACs, while those due to $H_D^C$ are also noticed. Both sets are shifted by $H_D^L$ to higher fields. The $H_{SIA}^D$ term is able to shift higher energy ACs to slightly smaller fields. The remarkable feature of the simultaneous inclusion of all SO terms is that ACs related to distinct $n$ values are grouped at different values of critical fields.

50 meV) at the same critical field as the ACs involving $n=0$ levels; in the latter, the existence of only one crossing at low fields in the second shell displaces the AC between $\{0,1,-1\}$ and $\{1,0,+1\}$ to a higher field and energy. For this same reason, the ACs at 1 T due to $H_D^C$ and visible in Fig. 5 no longer occurs in the full $H$.

In the next two figures we consider a QD defined by distinct values from those in Table II. In Fig. 9 we consider a wider well QD by using a doubled $z_0$ size, which is equivalent to reducing the influence of the linear BIA term in the system. As expected, the spectrum becomes very similar to that one of Fig. 4, where only SIA terms are included. Notice that the first AC is shifted back to $B_C \simeq 2.55$ T (panel B and insets of panels C and D), and every $H_R$-induced AC occurs again around this critical field (panels C and D), since the $H_D^L$ contribution is no longer strong enough to dislocate and group ACs involving states with different $n$ values. However, as $H_D^L$ is not zero, the range of critical fields around $B_C$ is wider than in Fig. 4. The ACs seen in panels C and D around 1 and 5 T are again related to the small influence of the $H_D^C$ term.

In Fig. 10 we simulate the case where the zero-field splittings are cancelled even in the presence of all SO terms, which is reasonably obtained by taking an interfacial field $dV/dz$ four times stronger than in Table II; this clearly enhances the influence of the Rashba term $H_R$ in the system. Notice in panels A and B that not only the zero-field splittings reasonably vanish, but also that the Zeeman splittings

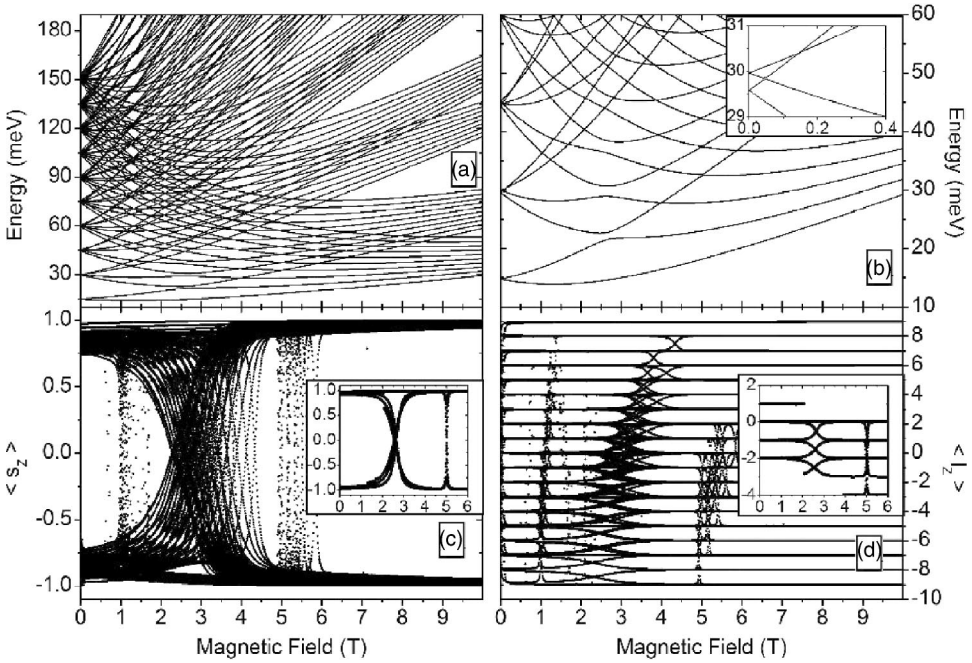


FIG. 9. Full $H$ spectrum of an InSb QD with doubled $z_0$ size (other parameters as in Table II). Because of the reduction of $H_D^L$ influence, the spectrum shows very similar features to the ones seen in Fig. 4, even though a wider range of critical fields is present here.

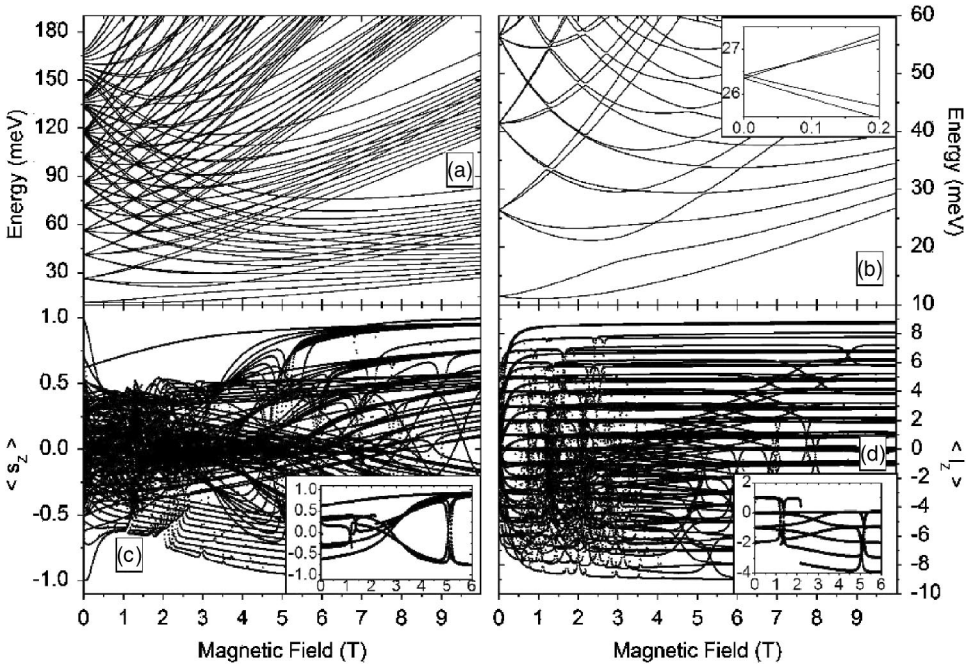


FIG. 10. Full $H$ spectrum of an InSb QD with four times stronger Rashba field $dV/dz$ (other parameters as in Table II). Notice the cancellation not only of the zero-field energy splittings but also of the spin splittings at low fields (panels A and B). Under such stronger Rashba coupling, the set of ACs related to the $H_D^C$ selection rules becomes visible around 1.1 T (panel B and insets of panels C and D), while $B_C$ for the first AC is shifted back to about 2.7 T, the same occurring for the ACs around 5 T due to $H_D^C$. Notice also the enormous state mixture in panel C. At zero field, most states have $|\langle s_Z\rangle| < 0.5$, except for the ground state (inset), with $|\langle s_Z\rangle| \simeq 0.7$.

are practically suppressed at low fields ($B_0 \lesssim 1.5$ T). At zero magnetic field, an energy shell structure identical to that of the pure $H_0$ (Fig. 1) is formed but displaced to smaller energies, with the same level separation of 15 meV. In the inset of panel B one sees that the energy of the $j=3/2$ level is reduced to the one of $j=1/2$, going from 30 to 26.5 meV (compare with the same inset of Fig. 8). While the zero-field splittings vanish, on the other hand, the energy gaps opened at the ACs are even bigger, as seen in panel B. In addition, the critical field is moved back to $B_C \simeq 2.7$ T, close to the value of 2.55 T of Fig. 4, where no BIA terms are included; the same occurs for the AC due to $H_D^C$, which has moved back to $\simeq 5$ T; that is, the value in Fig. 5. The rearrangement of electronic levels is so remarkable that the other set of ACs related to the cubic BIA term become visible at $\simeq 1.1$ T (compare insets of panels C and D in this figure with the ones in Figs. 5 and 8), involving the states $\{0,1,-1\}$ and $\{0,-2,+1\}$, as well as $\{1,0,-1\}$ and $\{0,-3,+1\}$, and visible in panel B at 33 and 44 meV, respectively. One must emphasize that even though the electronic levels disperse less than in Fig. 8, the SO-induced state mixture is much stronger and it is no longer possible to define narrow ranges of critical fields for higher energy ACs, as visible in panels C and D. Notice also that even at low fields, the lowest QD levels have $|\langle s_Z\rangle| < 0.5$, only the ground state having $|\langle s_Z\rangle| \simeq 0.7$.

### D. QD size dependence

Although decreasing the influence of $H_D^L$ may, in principle, seem similar to increasing the influence of $H_R$ in the system, observe that Figs. 9 and 10 are totally different, showing the intricate competition between the possible SO terms in the definition of the electronic properties of narrow-gap QDs. Comparison of three of such properties—zero-field energy splittings, critical magnetic fields where ACs occur, and energy gaps opened at those ACs—is made in the next two figures. Figure 11(12) shows results as function of the QD lateral radius $l_0$ (vertical width $z_0$); in both figures, the left panel shows the zero-field splitting between states $j=3/2$ and $j=1/2$ of the second energy shell, the middle panel shows the critical magnetic field where the second and third QD lowest energy levels exhibit an AC, and the right panel shows the energy gap opened at such AC. In these two figures, curves having square, circle, and triangle as symbols refer, respectively, to a QD as defined in Table II, a QD with doubled $z_0$, and a QD with four times stronger $dV/dz$; the arrows at $l_0=190$ Å and $z_0=40$ Å indicate the QD dimensions for which the spectra of Figs. 1–8 were calculated, while the dotted line in the middle panels indicates the $B_C^0$ field as given in Eq. (20), where the first crossing of the pure FD levels $\{0,0,-1\}$ and $\{0,-1,+1\}$ occurs.

Starting with the zero-field splittings, one should remember that they are dominated by $H_D^L$ if a weak Rashba field is considered. Notice in Fig. 11 that they decrease by increasing $l_0$, going to 1.8 meV when $l_0=330$ Å ($\hbar\omega_0=5$ meV) for the parameters of Table II. Observe that such a drop is faster if one increases $z_0$ or $dV/dz$, almost cancelling the splitting when $l_0 > 250$ Å. The same behavior, and for the same reason, is observed with respect to $z_0$ in Fig. 12 for the parameters of Table II, where the splitting almost vanishes when $z_0 > 120$ Å; in this figure we also verify that if $dV/dz$ is made four times stronger in a $z_0=40$ Å QD, the splitting practically vanishes as discussed in Fig. 10, and increases

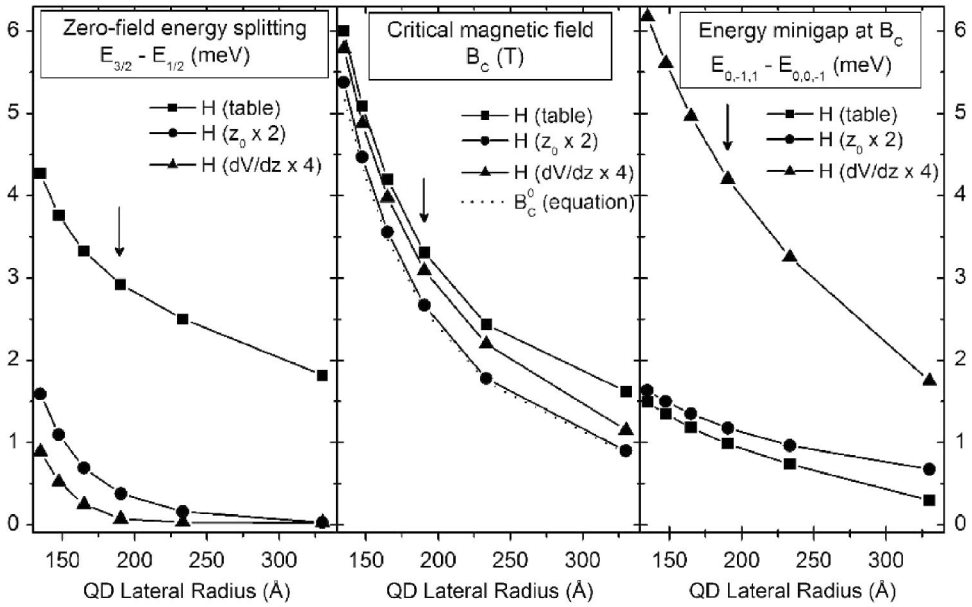


FIG. 11. Zero-field energy splittings for second energy shell states (left panel), critical magnetic fields for the lowest level AC (middle panel), and energy gaps opened at that AC (right panel) as function of the QD lateral radius $l_0$. Squares, circles, and triangles indicate, respectively, a QD defined by parameters in Table II, a QD having doubled $z_0$, and a four times stronger $dV/dz$. Dotted line shows $B_C^0$ as per Eq. (20). Arrows at $l_0=190$ Å show QD radius where spectra from Figs. 1–8 were calculated.

with $z_0$ until saturation at 2.6 meV for $z_0>100$ Å. To produce cancellation of level splittings, authors in Ref. 6 cite the possibility of achieving this in a 2DEG by including only $H_D^L$ and $H_R$ contributions; however, the inclusion of $H_D^C$ and $H_{SIA}^D$ terms is also necessary in order to get precise values in narrow-gap QDs. In our InSb QDs, for example, the needed values of $z_0$ or $dV/dz$ for such cancellation are about 10% smaller than those obtained by considering only $H_D^L$ and $H_R$.

Regarding the critical fields where ACs occur, we have seen that they are mostly determined by $H_R$ (for the pair of levels considered) and have values close to $B_C^0$ when BIA terms are not present; the inclusion of $H_D^L$ is able to shift $B_C$ to higher fields. Observe in Fig. 11, for the parameters of Table II, that $B_C$ decreases by increasing $l_0$ in a similar way to $B_C^0$ as given in Eq. (20) (dotted line). Increasing the field $dV/dz$ produces sizeable changes only at larger radii; at $l_0=330$ Å, for example, $B_C$ goes from 1.6 to 1.1 T. As expected, by increasing $z_0$, $B_C$ becomes practically identical to $B_C^0$. Notice in this figure that critical fields lower than 1 T are feasible; effects at such low fields are perhaps easier to verify experimentally. It is clear in Fig. 12 that, depending on the field $dV/dz$, $B_C$ saturates at 2.5 or 2.6 T (close to $B_C^0$, dotted line) when $z_0>100$ Å. Now it is interesting to make a comparison of our results with the ones from Ref. 32, where an InSb QD with $l_0=270$ Å ($\hbar\omega_0=7.5$ meV) was considered without taking into account BIA terms, and $B_C\simeq 1.7$ T was

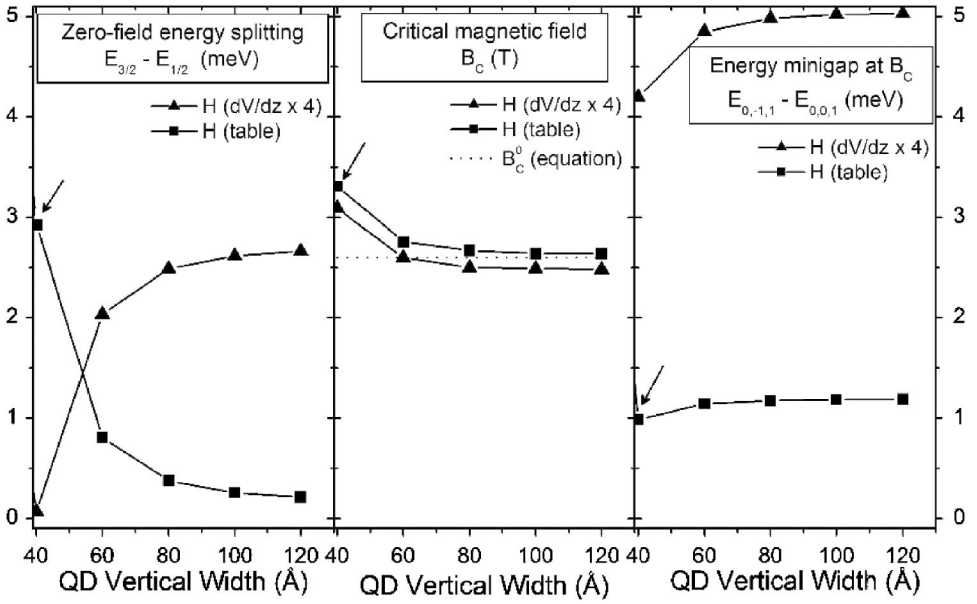


FIG. 12. Zero-field energy splittings for second energy shell states (left panel), critical magnetic field for the lowest level AC (middle panel), and energy gaps opened at that AC (right panel) as function of the QD vertical width $z_0$. Squares and triangles indicate, respectively, a QD defined by parameters in Table II, and a QD having a four times stronger Rashba field $dV/dz$. The dotted line shows $B_C^0$ as per Eq. (20). Arrows at $z_0=40$ Å show QD width where spectra from Figs. 1–8 were calculated.

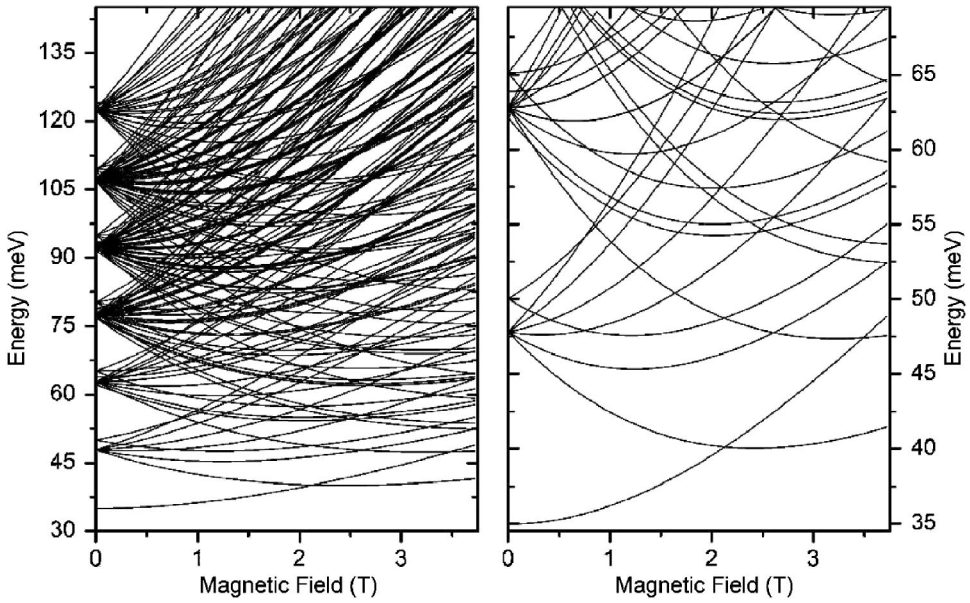


FIG. 13. Two interacting particle QD spectrum when no SO terms are taken into account in Eq. (19). The left panel shows every state obtained from the numerical diagonalization, while the right panel shows a zoom focusing on the singlet ground state and on the zero-field splittings as induced by the exchange energy for the lowest excited states.

found. At $l_0=270$ Å in Fig. 11, one sees that the critical field decreases from 2.1 to 1.8 and then to 1.5 T by, respectively, increasing $dV/dz$ and $z_0$; this last value is the one in our calculations that better simulates Ref. 32, since the $H_D^L$ influence is almost negligible. The 0.2 T difference is probably due to the fact that such reference takes into account nonparabolicity effects of the InSb conduction band which can, in fact, shift $B_C$ to a slightly higher field.

For the gap opened at the AC occurring at $B_C$, the main contribution comes from the Rashba term (for the pair of levels considered). Notice in Fig. 11 that the gap decreases by increasing the QD lateral radius; an enhancement in $dV/dz$ drastically widens the gap, that goes from 1 to 4.2 meV at $l_0=190$ Å, for example; the influence of a larger $z_0$ seems important only at larger radii. Observe in Fig. 12 the enhancement of the gap with $z_0$ until it saturates at around $z_0=100$ Å. Notice again the enormous enhancement of the energy gap opened at this AC if a larger Rashba field $dV/dz$ is considered.

A measurement of the quantities in Figs. 11 and 12 in similar samples would be able, in principle, to yield better estimates for the $\alpha$ and $\gamma$ SO coupling parameters, and provide experimental bounds to the broad range of values available in the literature for nominally the same material.

## V. RESULTS FOR TWO-ELECTRON QDS

After having described in detail the one-particle QD problem, we are now in a position to deal with the two interacting electron problem. The QD defining parameters are again given in Table II, and we have opted to not detail the isolated influence of each of the SO terms. The construction of the antisymmetrized two-particle states includes 20 one-particle orbitals having $|l|\leqslant 3$ and $n\leqslant 1$ (they complete the first four energy shells at zero field of $H_0$), amounting to 190 possible two-particle states that can be labeled, in the absence of SO interactions, by the projections of orbital $M_L$ and spin $M_S$ total angular momenta, as already mentioned. When SO coupling is included (full $\widetilde{H}$), in analogy with the single-particle problem, one can define the expectation values of the total spin operator as $\langle S_Z\rangle$ and of the corresponding total angular momentum as $\langle M_Z\rangle$.

Figure 13 shows the two interacting particle QD spectrum without SO couplings; that is, in Eq. (19) one assumes $H=H_0$. If the two electrons inside the QD were noninteracting, we would have, at zero field, energy shells between 30 and 120 meV, separated again by 15 meV; under a magnetic field, states having negative $M_L$ and positive $M_S$ (again because of the InSb negative $g$-factor) would acquire smaller energy. The presence of Coulomb interaction, however, shifts those shells to higher energies, and also introduces zero-field splittings in the spectrum. Although the left panel shows all states obtained from the numerical diagonalization, it is the zoom in the right panel that yields a better appreciation of the interacting QD levels. If only the direct Coulomb energy were effective (by not taking into account the antisymmetric nature of the QD wave functions), the zero-field energies would be shifted up by about 5 meV; in such a case, the ground state (two electrons in the first $H_0$ shell) would be at 35 meV, the first excited shell (one electron in the first and other in the second $H_0$ shell) at 50 meV, and the second excited shell (one electron in the first and other in the third, or two electrons in the second $H_0$ shell) at 65 meV. However, the presence of the exchange Coulomb energy is able to break apart the degeneracy of states at zero field—except obviously for the singlet ground state—and induce splittings in the spectrum, even with no SO interaction. For example, notice the first excited energy shell: while two singlets remains at 50 meV, two triplets are shifted down by the exchange contribution to 47.5 meV (the singlet ground state remains at 35 meV). A small magnetic field ($\lesssim$0.1 T) yields the normal sequence of QD states for increasing energy: $\{M_L,M_S\}=\{0,0\}$ for the singlet ground state; $\{-1,1\}$, $\{-1,0\}^T$, $\{-1,-1\}$, $\{1,1\}$, $\{1,0\}^T$, $\{1,-1\}$ for the first excited triplets; and $\{-1,0\}^S$, $\{1,0\}^S$ for the first excited singlets, where the superscripts $S/T$ have obvious meaning. For the following discussion, it is useful to remark three features: the

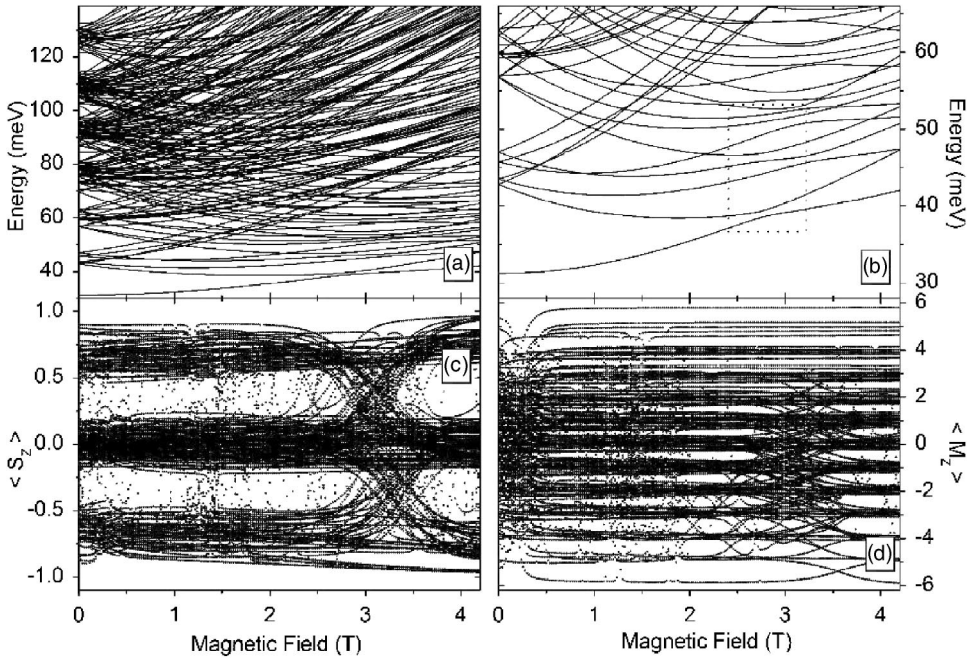


FIG. 14. Two interacting particle QD spectrum when all possible SO terms are taken into account in Eq. (19). Comparing the ground and first excited states in panel B with those in right panel of Fig. 13, one can see that SO energy acts against the direct Coulomb term and favors the exchange electron-electron interaction. The first excited triplets, at zero field, are split according to the $M_J$ values. ACs at around 3 T [panels $C$ ($\langle S_Z\rangle$) and $D$ ($\langle M_Z\rangle$)] are due to the Rashba term; the lowest ACs are indicated by the rectangle in panel B, detailed on Fig. 15.

lowest level crossing occurs at $B_C^{0(2e)}=2.1$ T involving the states $\{0,0\}$ and $\{-1,1\}$; at 0.75 T, $\{-1,0\}^S$ becomes the fourth QD state, with energy that parallels the third state, $\{-1,0\}^T$; the two states $\{-1,0\}^{S/T}$ cross with the lowest state from the next energy shell, $\{-2,1\}$, respectively, at 2.1 and 2.6 T. The $B_0$ evolution of $\langle S_Z\rangle$ and $\langle M_Z\rangle$ values is not shown, as they are obviously pure states, taking only the integer values $-6\leqslant\langle M_Z\rangle\leqslant 6$ and $\langle S_Z\rangle=0,\pm 1$ at any field.

Figure 14 shows the QD spectrum obtained by considering the full two-particle Hamiltonian $\widetilde{H}$ of Eq. (19). One may identify in panel A similar features to the one-electron case; for example, the linear Dresselhaus term almost destroys the energy shell structure at zero field by shifting level crossings and inducing new zero-field splittings, while the Rashba term introduces level ACs and opens energy gaps in the spectrum. It is in panel B that one can appreciate more details of the competition between Coulomb and SO interactions in the narrow-gap QD spectra. Observe that the SO interaction, at zero field, acts against the direct Coulomb term and, essentially, favors the effect of exchange; the ground state, for example, is shifted back from 35 (Fig. 13) to 31 meV, close to the noninteracting value of 30 meV, while the first excited shell starts with energies even lower than its noninteracting value of 45 meV, within the range of 43 to 47 meV. Other important feature can be seen, for example, in this first excited shell, where the original triplets are broken into their three possible components according to the projection of the total angular momentum, $M_J=M_L+M_S$. Notice that, at zero field, such components are the states $\{-1,1\}$ and $\{1,-1\}$ ($M_J=0$), $\{-1,0\}^T$ and $\{1,0\}^T$ ($|M_J|=1$), $\{-1,-1\}$ and $\{1,1\}$ ($|M_J|=2$), with increasing energy, while the ground ($\{0,0\}$, $M_J=0$) and first excited ($\{-1,0\}^S$ and $\{1,0\}^S$, $|M_J|=1$) singlets remain the same. At finite field, one sees that ACs due to $H_R$ occur at around 3 T, as evident in panels C and D. The first AC is between states $\{0,0\}$ and $\{-1,1\}$ at $B_C^{(2e)}=2.7$ T, so that the difference between $B_C^{(2e)}$ and $B_C^{0(2e)}$ ($\sim$0.6 T) is basically the same as between $B_C$ and $B_C^0$ ($\sim$0.7 T) for the one-electron problem; this means that the critical field shift caused by $H_D^L$ on this AC appears not to be affected by the QD occupation, even though the critical fields themselves are decreased by such occupation. Whether such a result is valid for higher occupations and also for other parameters is still a point under investigation. That crossing at 0.75 T (Fig. 13) involving the state $\{-1,0\}^S$ now occurs at around 1 T, and those two states $\{-1,0\}^{S/T}$ now exhibit ACs with the state $\{-2,1\}$ at fields of 2.6 and 3.2 T, respectively, instead of the crossings at 2.1 and 2.6 T of the previous figure. The ACs visible in the rectangle of panel B, as well as in panels C and D, are again due to the Rashba term and are displaced by the linear BIA term to higher fields.

To clarify the two lowest ACs, we show in Fig. 15 the $B_0$ evolution of $\langle S_Z\rangle$ and $\langle M_Z\rangle$ values for the states indicated in the rectangle of panel B of Fig. 14. Panels A and B include the ten QD lowest energy levels, while panels A1 and B1 (A2 and B2) separately show the 2 (3) states that participate in the first (second) AC occurring at around 39 (46) meV; labels 1 to 5 indicate the level sequence in increasing energy. The AC between states 1 and 2 ($\{0,0\}$ and $\{-1,1\}$) clearly occurs at $B_C^{(2e)}=2.7$ T. The AC involving states 3, 4, and 5 ($\{-1,0\}^T$, $\{-1,0\}^S$, and $\{-2,1\}$) has distinct features; notice that first a mixture between states 4 and 5 occurs at 2.6 T, followed by another mixture at 3.2 T involving states 4 and 3. In this way, state 4 acts as an intermediary of two ACs, and the $\langle S_Z\rangle$ and $\langle M_Z\rangle$ values of such state, before and after this region of critical fields, are conserved (exchanged twice); this gives the appearance of only one effective AC between states 3 and 5. These ACs obey a selection rule $\Delta M_L=\pm 1=-\Delta M_S$ similar to that of the one-particle Rashba problem. As discussed for the one-electron problem, when the parameters of Table II are used, the influence of the cubic Dresselhaus term is small on the opening of gaps in the spectrum; its selection rule becomes $\Delta M_L=\mp 3$ and $\Delta M_S=\pm 1$, and the first possible ACs due to $H_D^C$ involve the states

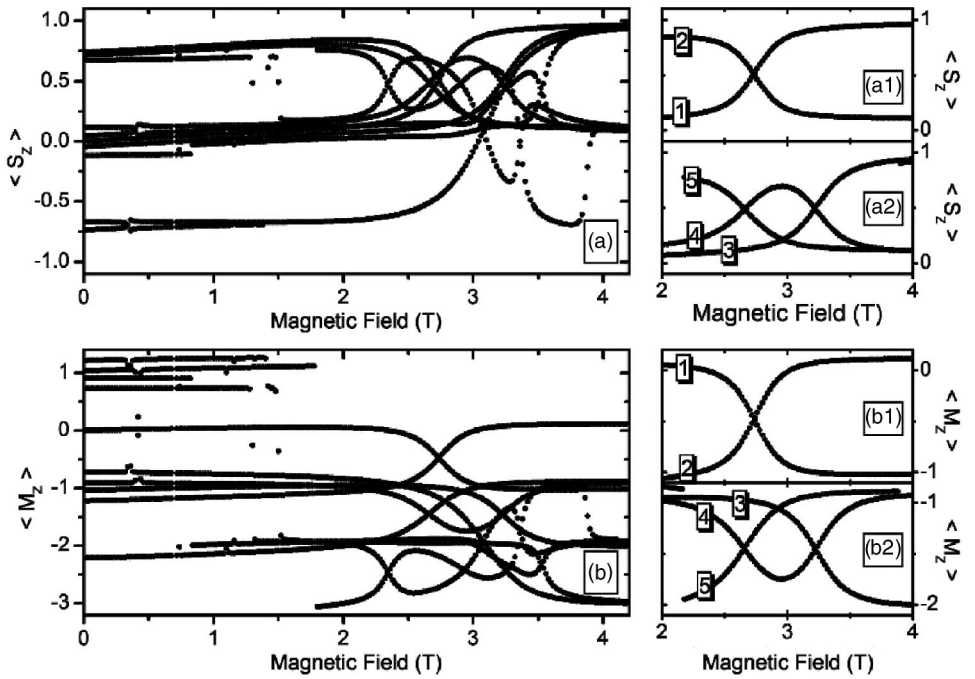


FIG. 15. $B_0$ dependence of $\langle S_Z\rangle$ (upper panels) and $\langle M_Z\rangle$ (lower panels) values for the lowest ACs shown in the rectangle of panel B in Fig. 14. Panels A and B include all the ten states present in that rectangle. The right panels include only the five lowest states, labeled by their ordering in increasing energy: panels $A_1$ and $B_1$ are related to the first AC between states 1 and 2, while panels $A_2$ and $B_2$ are related to the next two ACs. Although it appears that only one AC between states 3 and 5 is effective, state 4 acts as an intermediate state for this three-state mixture.

$\{-2,1\}$ and $\{1,0\}^{S/T}$. Similarly to what happens with the one-particle case, they become visible in the spectrum for higher interfacial fields $dV/dz$.

A very important difference between the one- and two-particle problems must be emphasized. While in a one-particle QD there is no AC involving its ground state, notice that the lowest energy AC in a two-particle QD does involve its ground state, and is related to a *singlet-triplet mixture*. Observe also that the critical magnetic field where this first AC occurs decreases by increasing the QD occupation, going from $B_C$=3.3 T to $B_C^{(2e)}$=2.7 T; in Ref. 32 (where different QD parameters are used), it goes from 1.7 to 1 T, which yields basically the same field variation, and the small difference may again be attributed to the conduction band nonparabolicity effects considered in that reference. One should remember from Eq. (20) that such critical fields may be reduced by decreasing the QD confinement energy. The strong intrinsic (i.e., no-phonon-assisted) singlet-triplet mixture involving the QD ground state at low magnetic fields can, in principle, be explored in the implementation of quantum computing devices, as one could envision state swapping (rotation) of the two-electron QD controlled by an external magnetic field.[44]

## VI. CONCLUSIONS

We have analyzed in detail the influence of different SO mechanisms originating from both surface and bulk inversion asymmetries in the FD spectrum of parabolic zinc-blende narrow-gap QDs. We have shown that the SIA Hamiltonian is decomposed in two $k$-linear contributions—one diagonal and the other the so-called Rashba term, while the BIA Hamiltonian is also separated in two contributions: one $k$-linear and the other $k$-cubic. We have seen that $H_{SIA}^D$ introduces small zero-field energy splittings; $H_R$ produces strong state mixtures and level ACs at critical magnetic fields that depend on QD parameters; $H_D^C$ has relatively small influence for a certain range of QD parameters; and $H_D^L$ induces large state admixture (mainly at low fields) but without introducing ACs in the low energy FD spectrum. When all SO contributions are taken into account in the diagonalization, we have seen that $H_D^L$ shifts the critical fields of $H_R$-produced ACs to higher fields, and it is also able to group ACs related to the same $n$ value. We have shown that when the interfacial field $dV/dz$ is larger, a number of features appear in the spectrum: the zero-field energy splittings can be made to vanish, the spin splitting is cancelled at low fields, ACs related to $H_D^C$ selection rules arise in the low energy spectrum, and a strong state mixture ($|\langle s_Z\rangle|<0.5$) is induced at close-to-zero magnetic fields even for the lowest energy states. The negative sign of the $g$-factor, as well as the relatively large value of the SO constants (in comparison with those in GaAs, for example), are essential for the appearance of such features.

For the two interacting electron QD problem, we have shown that the direct Coulomb interaction increases QD level energies, while the exchange interaction decreases them, as well as induces zero-field splittings in the spectrum. The SO interaction, in a sense, acts against the direct Coulomb while it favors exchange, and also creates zero-field splittings in the spectrum. The critical field where the lowest AC occurs decreases when compared with the one-particle

QD. The difference between this field and the lowest crossing without any SO coupling is basically the same as in the one-particle QD; the behavior under higher occupations is still to be investigated. An interesting fact that, in principle, could be better explored for qubit design is that, differently from what happens with the one-particle problem, the interacting QD ground state also exhibits AC, where strong intrinsic spin-flip processes occur. Such state rotation may have an easier experimental access given that the critical magnetic field be relatively low, especially for properly chosen QD material and parameters.

We conclude by drawing attention to the importance that the SO-induced energy splittings have on the spin lifetimes. Many schemes for quantum computing rely on a well-defined spin, so that careful attention has to be paid to phonon-assisted[13] or hyperfine[45] spin-flips. The *intrinsic* mixtures described here provide an inherent upper bound to the spin lifetime in QDs, given by $\tau_{SO}=\hbar/(2\pi\Delta)$, where $\Delta$ is the energy gap at the AC, tunable by changing the QD parameters (see Figs. 11 and 12). The application of magnetic fields could then produce undesirably small $\tau_{SO}$ in a given QD, which proper qubit design would have to address.

## ACKNOWLEDGMENTS

We acknowledge support from FAPESP-Brazil, US DOE Grant No. DE-FG02-91ER45334, and the CMSS Program at OU.

[1] D. K. Young, J. A. Gupta, E. Johnston-Halperin, R. Epstein, Y. Kato, and D. D. Awschalom, Semicond. Sci. Technol. **17**, 275 (2002).
[2] S. Datta and B. Das, Appl. Phys. Lett. **56**, 665 (1990).
[3] S. Das Sarma, J. Fabian, X. Hu, and I. Zutic, Superlattices Microstruct. **27**, 289 (2000).
[4] E. I. Rashba, J. Supercond. **15**, 13 (2002).
[5] S. A. Wolf, J. Supercond. **13**, 195 (2000).
[6] J. Schliemann, J. C. Egues, and D. Loss, Phys. Rev. Lett. **90**, 146801 (2003).
[7] D. Loss and D. P. DiVincenzo, Phys. Rev. A **57**, 120 (1998).
[8] S. Das Sarma, J. Fabian, X. Hu, and I. Zutic, Solid State Commun. **119**, 207 (2001).
[9] X. Hu and S. Das Sarma, Phys. Rev. A **64**, 042312 (2001).
[10] N. S. Averkiev, L. E. Golub, and M. Willander, Semiconductors **36**, 91 (2002).
[11] J. Fabian and S. Das Sarma, J. Vac. Sci. Technol. B **17**, 1708 (1999).
[12] A. V. Khaestkii and Y. V. Nazarov, Phys. Rev. B **61**, 12639 (2000).
[13] A. V. Khaestkii and Y. V. Nazarov, Phys. Rev. B **64**, 125316 (2001).
[14] E. A. A. Silva, G. C. La Rocca, and F. Bassani, Phys. Rev. B **55**, 16293 (1997).
[15] T. Hassenkam, S. Pedersen, K. Baklanov, A. Kristensen, C. B. Sorensen, P. E. Lindelof, F. G. Pikus, and G. E. Pikus, Phys. Rev. B **55**, 9298 (1997).
[16] E. A. A. Silva, G. C. La Rocca, and F. Bassani, Phys. Rev. B **50**, 8523 (1994).
[17] F. G. Pikus and G. E. Pikus, Phys. Rev. B **51**, 16928 (1995).
[18] S. Gopalan, J. K. Furdyna, and S. Rodriguez, Phys. Rev. B **32**, 903 (1985).
[19] G. Dresselhaus, Phys. Rev. **100**, 580 (1955).
[20] Y. A. Bychkov and E. I. Rashba, J. Phys. C **17**, 6039 (1984).
[21] I. L. Aleiner and V. I. Fal'ko, Phys. Rev. Lett. **87**, 256801 (2001).
[22] J. B. Miller, D. M. Zumbühl, C. M. Marcus, Y. B. Lyanda-Geller, D. Goldhaber-Gordon, K. Campman, and A. C. Gossard, Phys. Rev. Lett. **90**, 076807 (2003).
[23] M. Valín-Rodríguez, A. Puente, and L. Serra, Phys. Rev. B **66**, 045317 (2002).
[24] M. Valín-Rodríguez, A. Puente, L. Serra, and E. Lipparini, Phys. Rev. B **66**, 165302 (2002).
[25] M. Valín-Rodríguez, A. Puente, L. Serra, and E. Lipparini, Phys. Rev. B **66**, 235322 (2002).
[26] M. Governale, Phys. Rev. Lett. **89**, 206802 (2002).
[27] M. Cardona, N. E. Christensen, and G. Fasol, Phys. Rev. B **38**, 1806 (1988).
[28] C. Sikorski and U. Merkt, Phys. Rev. Lett. **62**, 2164 (1989).
[29] W. Zawadzki and M. Kubisa, Semicond. Sci. Technol. **8**, S240 (1993).
[30] P. Junker, U. Kops, U. Merkt, T. Darnhofer, and U. Rössler, Phys. Rev. B **49**, 4794 (1994).
[31] E. Alphandéry, R. J. Nicholas, N. J. Mason, S. G. Lyapin, and P. C. Klipstein, Phys. Rev. B **65**, 115322 (2002).
[32] T. Darnhofer and U. Rössler, Phys. Rev. B **47**, 16020 (1993).
[33] O. Voskoboynikov, C. P. Lee, and O. Tretyak, Phys. Rev. B **63**, 165306 (2001).
[34] V. Fock, Z. Phys. **47**, 446 (1928).
[35] C. G. Darwin, Proc. Cambridge Philos. Soc. **27**, 86 (1931).
[36] L. Jacak, A. Wojs, and P. Hawrylak, *Quantum Dots* (Springer, Berlin, 1998).
[37] G. Arfken, *Mathematical Methods for Physicists* (Academic, Orlando, 1985).
[38] C. F. Destefani, S. E. Ulloa, and G. E. Marques, Phys. Rev. B **69**, 125302 (2004).
[39] C. F. Destefani, Ph.D. dissertation, Universidad Federal de Sao Carlos (2003).
[40] L. M. Woods, T. L. Reinecke, Y. Lyanda-Geller, Phys. Rev. B **66**, 161318 (2002).
[41] Some typos were found in the expressions for $H_D^L$ and $H_D^C$ of our previous work (Ref. 38) and corrected here. The results shown there, however, were obtained by the correct expressions.
[42] R. N. Zare, *Angular Momentum: Understanding Spatial Aspects in Chemistry and Physics* (Wiley, New York, 1988).
[43] J. J. Sakurai, *Modern Quantum Mechanics* (Addison-Wesley, New York, 1995).
[44] *Semiconductor Spintronics and Quantum Computing*, edited by D. D. Awschalom, D. Loss, and N. Samarth (Springer, New York, 2002).
[45] A. Khaetskii, D. Loss, and L. Glazman, Phys. Rev. B **67**, 195329 (2003).